

Charge Transfer Complex of N-(4-methoxyphenyl)-2-oxooxazolidine-3-sulfonamide and Picric Acid: Experimental and DFT Studies

Karim Dinar^{1,2*}, Mekki Kadri² and Achour Seridi²

¹Echahid Cheikh Larbi Tebessi University - Tebessa - Constantine road, 12002, Tebessa, Algeria

²Physical Chemistry Laboratory, 08 Mai 45 University, BP401, Guelma. 24000. Algeria

*Corresponding author (e-mail: dinar.karim@umc.edu.dz)

The formation of a charge-transfer (CT) complex between the electron donor: N-(4-methoxyphenyl)-2-oxooxazolidine-3-sulfonamide (SOZ) and the acceptor molecule: picric acid (PiOH) with a 1:1 stoichiometry ratio in dichloromethane and chloroform at room temperature was studied using spectrophotometry. Various parameters were calculated and the polarity effects on these parameters were considered. IR spectroscopy confirmed the presence of different functional groups in the complex. The experimental results were supplemented by quantum calculations, Density Functional and Time-Dependent Functional Theories (DFT and TD-DFT) at the B3LYP level. Theoretical UV-visible and simulated IR spectra were obtained using B3LYP/6-311G(d,p) and compared with experimental results. Mulliken charge, MEP, HOMO and LUMO energy values were calculated, and NBO analysis was performed on the optimized charge transfer complex.

Keywords: N-(4-methoxyphenyl)-2-oxooxazolidine-3-sulfonamide; picric acid; charge transfer complex; TD-DFT; HOMO-LUMO; MEP

Received: June 2022; Accepted: September 2022

Charge-transfer (CT) complexation is an important field of research. The formation of a charge transfer complex has been used to characterize derivatives as well as to calculate electron affinities and ionization potentials.¹⁻⁷ The interactions between these molecules play a significant role in many areas such as organic and inorganic reactions, biological processes and the design of photoelectric products.⁸⁻¹¹

To understand protein folding and control the macromolecular assembly, we have to understand the thermodynamics and behaviour of complex formation.¹²⁻¹⁴

The properties of CT complexes formed using acceptor molecules with donors containing oxygen, nitrogen and sulfur atoms, have been of increasing importance in recent years.⁹⁻²² Among them are N-sulfamoyloxazolidinones which combine two pharmacophores, the sulfamoyl and the oxazolidinone moieties.^{23,24} These have been widely used against a large family of Gram-positive bacteria and as precursors in the synthesis of 2-chloroethylnitrososulfamides that have been used in chemotherapy as anti-tumour agents.^{25, 26}

In connection with our interest in studying charge transfer complexes,²⁷ we investigated CT complexes formed between a N-sulfamoyloxazolidinone compound, N-(4-methoxyphenyl)-2-oxooxazolidine-3-sulfonamide (SOZ), and picric acid.

The objective of the first part of the present work was to study the thermodynamics of the complexation reaction between donor and acceptor in the liquid phase and in the solid state by spectroscopic methods.

Different thermodynamic parameters such as the stability constant (K), standard thermodynamic reaction quantities (ΔH° , ΔG° , ΔS°), molar extinction coefficient (ϵ_{CT}), oscillator strength (f), transition dipole moment (μ_{EN}) and ionization potential (I_D) were calculated using spectrophotometric measurements in chloroform and dichloromethane, while IR spectroscopy was used to characterize the synthesized solid complexes.

In the second part of this work, we compared the experimental results with those obtained by quantum chemical calculations such theoretical UV-visible and IR absorbance spectra using the TD-DFT (Time-Dependent Density Functional Theory) method at the B3LYP level.

EXPERIMENTAL DETAILS

N-(4-methoxyphenyl)-2-oxooxazolidine-3-sulfonamide was synthesized according to a previously published method.²⁸ Picric acid (Aldrich) was used without further purification because of its high purity. The spectroscopic grade solvents (chloroform and

dichloromethane) were purchased from Prolabo and Fluka.

The UV-visible spectra were recorded between 400 nm and 220 nm using a Jasco UV-530 spectrophotometer equipped with a Jasco EHC-477S thermostat (± 0.1 °C) and 1.0 cm matched quartz cells. The IR spectra of the formed complexes and reactants were analysed in the form of KBr pellets using a spectrophotometer (Spectrum One Perkin Elmer FT-IR).

The solid CT complexes were prepared by separately dissolving equal amounts of the acceptor and donor at room temperature in the minimum volume of chloroform. The two solutions were combined and stirred for 24 hours.²⁹ The solid precipitate was filtered, washed many times with a minimum volume of chloroform, and dried under vacuum over anhydrous CaCl_2 .

Computational Details

The optimized structures of SOZ, PiOH and their CT complex were obtained using the Gaussian 09 package,³⁰ at the DFT/ B3LYP/6-311G (d, p) level of the theory. Two geometries of the formed CT complex were considered. In the first one (parallel model), the phenyl ring of PiOH was placed in parallel with the phenyl ring of SOZ. In the second one (T-shape model), the phenyl moiety of PiOH was placed perpendicular to the middle of the SOZ molecule. The most stable structure of the CT complex corresponds to the lowest binding energy.^{31,32}

The binding energy (E_{bind}) is defined as the difference of energies between the complex $E(\text{complex})^{opt}$ and its individual components, $E(\text{Donor})^{opt}$ and $E(\text{Acceptor})^{opt}$, in their optimized geometry:³³

$$E_{bind} = E(\text{complex})^{opt} - [E(\text{Donor})^{opt} + E(\text{Acceptor})^{opt}] \quad (1)$$

E is the absolute energy (the heat formation as reported by Gaussian).

Furthermore, TD-DFT calculations were also performed at the same level (B3LYP) in vacuum and in the PCM model, using two solvents with distinct dielectric constants (dichloromethane and chloroform) to study the electronic properties.³⁴

RESULTS AND DISCUSSION

1. Electronic Spectra

The formation of the SOZ-PiOH complex in solution was visualized by UV-vis spectrophotometry at 20 °C. As shown in **Fig. 1**, the UV-Visible spectrum of SOZ was different in the presence of the PiOH molecule. The intensity of the SOZ absorbance at 334 nm increased with the cumulative addition of PiOH in chloroform (10^{-3}M) and a new band was detected at 408 nm. In addition, two isosbestic points were recorded, at 308 and 369 nm. These characteristics were clearly caused by the CT complex formation.

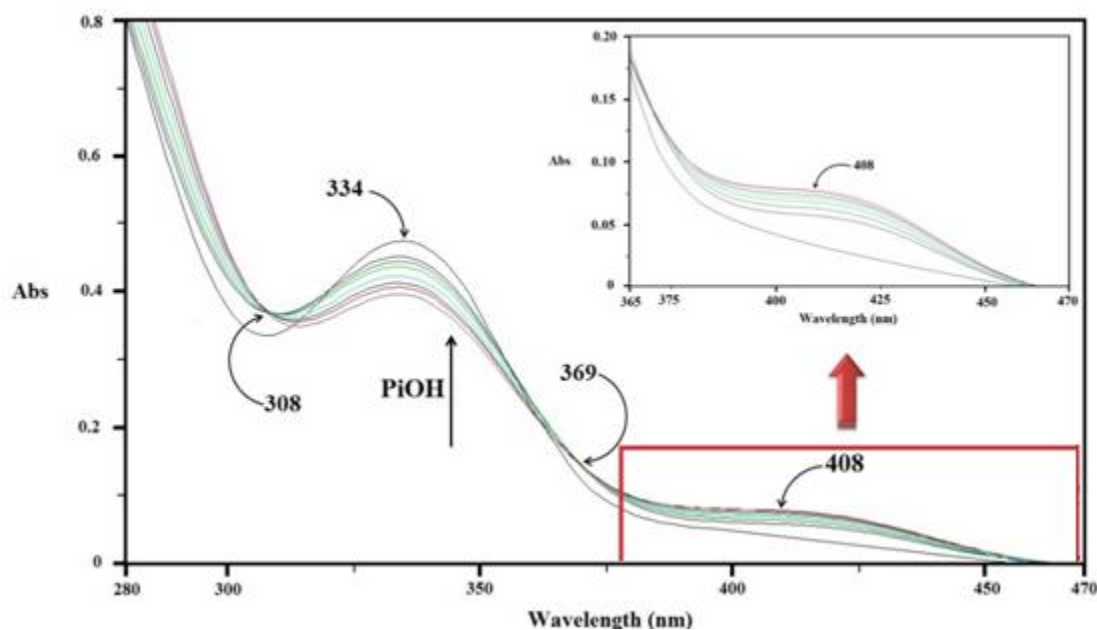


Figure 1. Absorption spectra of N-(4-methoxyphenyl)-2-oxooxazolidine-3-sulfonamide (2.5×10^{-4} M) with various concentrations of picric acid.

The presence of an isosbestic point in electronic spectra is good evidence that only two principal species are present in the reaction; in some electronic spectra, the existence of two isosbestic points is indicative of two chemical equilibria. This is the case in our study, which provides evidence of the presence of two CT complexes.

2. Determination of Stability Constants

The Benesi-Hildebrand equation was used to obtain the stability constants (K) and the molar extinction coefficients (ϵ_{CT}) for the 1:1 CT complexes in chloroform and dichloromethane at different temperatures (15-30 °C):³⁵⁻³⁷

$$\frac{[A]_0[D]_0}{Abs} = \frac{[D]_0}{\epsilon_{CT}} + \frac{1}{K\epsilon_{CT}} \quad (2)$$

With $Abs = d - d_A^0 - d_D^0$, $[D]_0$ and $[A]_0$ are the initial concentrations of the donor (SOZ) and the acceptor (PiOH) respectively. d is the absorbance of the mixture of PiOH and SOZ at some appropriate wavelength (λ_{CT}) against the solvent as reference and d_A^0 , d_D^0 are the absorbances of the PiOH and SOZ with the same concentrations as in the mixture, at the same wavelength. The quantity $\epsilon_{CT} = \epsilon - \epsilon_A - \epsilon_D$ refers to the correction of the molar extinction coefficient of the complex with those of the acceptor,

ϵ_A , and the donor, ϵ_D . Eq. (1) is valid under the condition $[D]_0 \gg [A]_0$ ³⁸. The plots of $[D]_0[A]_0/Abs$ versus $[D]_0$ were used to calculate the stability constant and molar extinction coefficient values at 15, 20, 25 and 30 °C in chloroform and dichloromethane (**Fig. 2**) and these are listed in **Table 1**. The correlation coefficients were greater than 0.98 for all such plots.

The stability constant values in dichloromethane were lower than those in chloroform; this indicates that the CT complex is more stable in a less polar solvent.³⁹

These complexes have large stability constants and molar extinction coefficients, which indicate that they are very stable, as expected: high donation of the SOZ molecule that holds N, O and S atoms.

3. Determination of Thermodynamic Parameters

The standard thermodynamic quantities (ΔH^0 , ΔS^0) associated with CT complex formation were evaluated from Van't Hoff plots,⁴⁰⁻⁴³ assuming ΔH^0 as constant over the temperature range of 20 – 35 °C.

The correlation coefficients for all plots of $\ln K$ vs. $\frac{1}{T}$ (**Fig. 3**) were greater than 0.97. The entropies and enthalpies of complexation were calculated using these plots.

Table 1. Stability constants K and molar extinction coefficients ϵ_{CT} of the 1:1 SOZ-PiOH complex in two solvents at different temperatures.

Solvent	T(K)	λ_{CT} (nm)	K_{CT}	ϵ_{CT} (L / mol.cm)	Linearity (R)
chloroform	288		4.32×10^4	14.40×10^3	0.99392
	293		1.11×10^4	20.42×10^3	0.99713
	298	408	0.32×10^4	30.77×10^3	0.99278
	303		0.20×10^4	45.54×10^3	0.99829
dichloromethane	288		1.60×10^4	0.92×10^3	0.99827
	293		0.83×10^4	1.23×10^3	0.99835
	298	331	0.35×10^4	1.55×10^3	0.99936
	303		0.17×10^4	3.43×10^3	0.98070

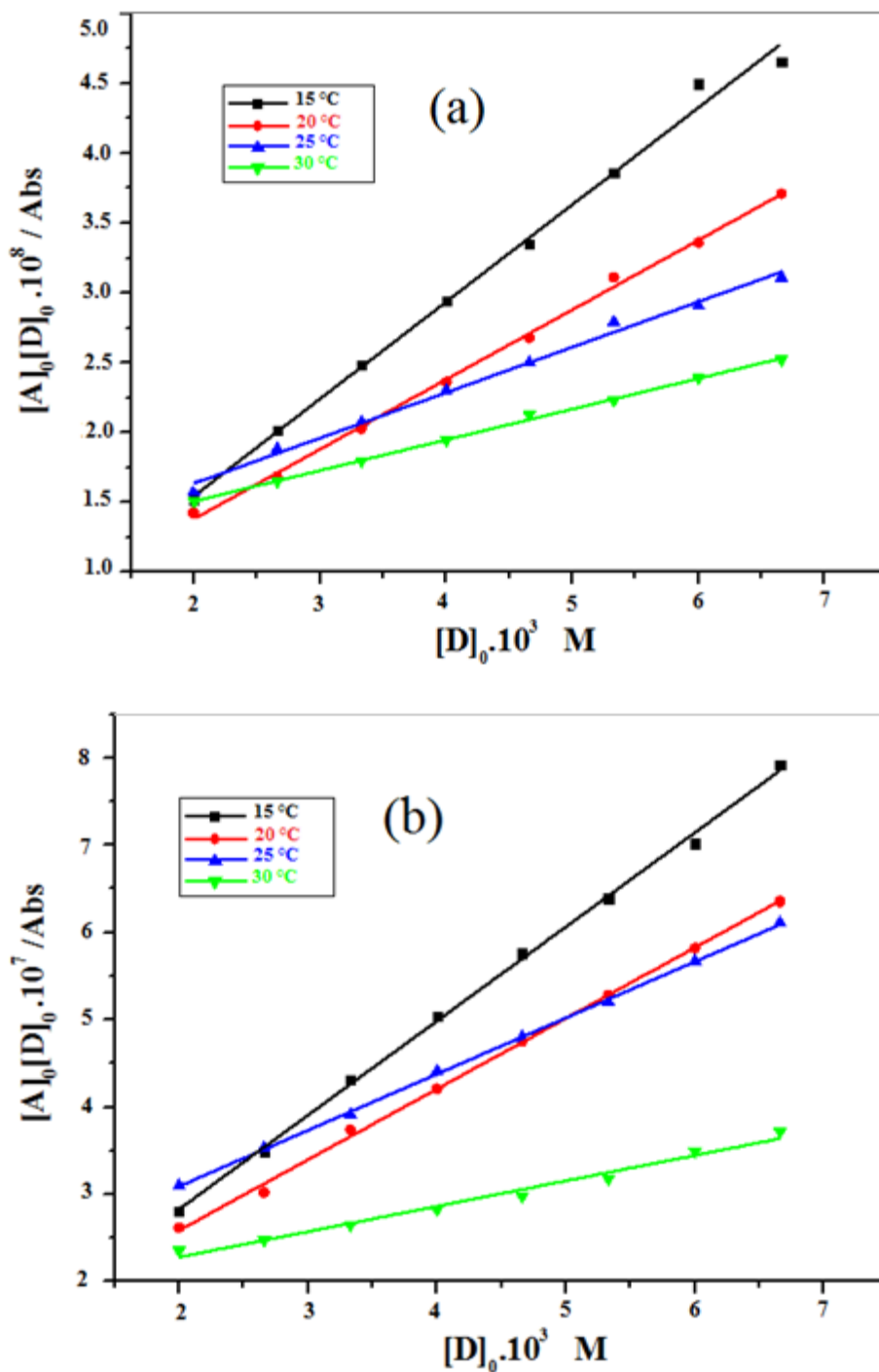


Figure 2. Benesi-Hildebrand plots for the SOZ- PiOH complex at 15, 20, 25 and 30 °C (a) in chloroform and (b) in dichloromethane.

The free energy (J/mol) was determined using the equation:

$$\Delta G^{\circ} = \Delta H^{\circ} - T\Delta S^{\circ} = -RT \ln K \quad (3)$$

where R is the gas constant ($8.314 \text{ J} \cdot \text{mol}^{-1} \cdot \text{K}^{-1}$) and T is the temperature in Kelvin.

The thermodynamic parameter values recorded in **Table 2** show that the CT reaction is thermo-dynamically favoured in both solvents, and it is an exothermic process. The enthalpy and entropy values were usually more negative as the stability constant of the complex increased.

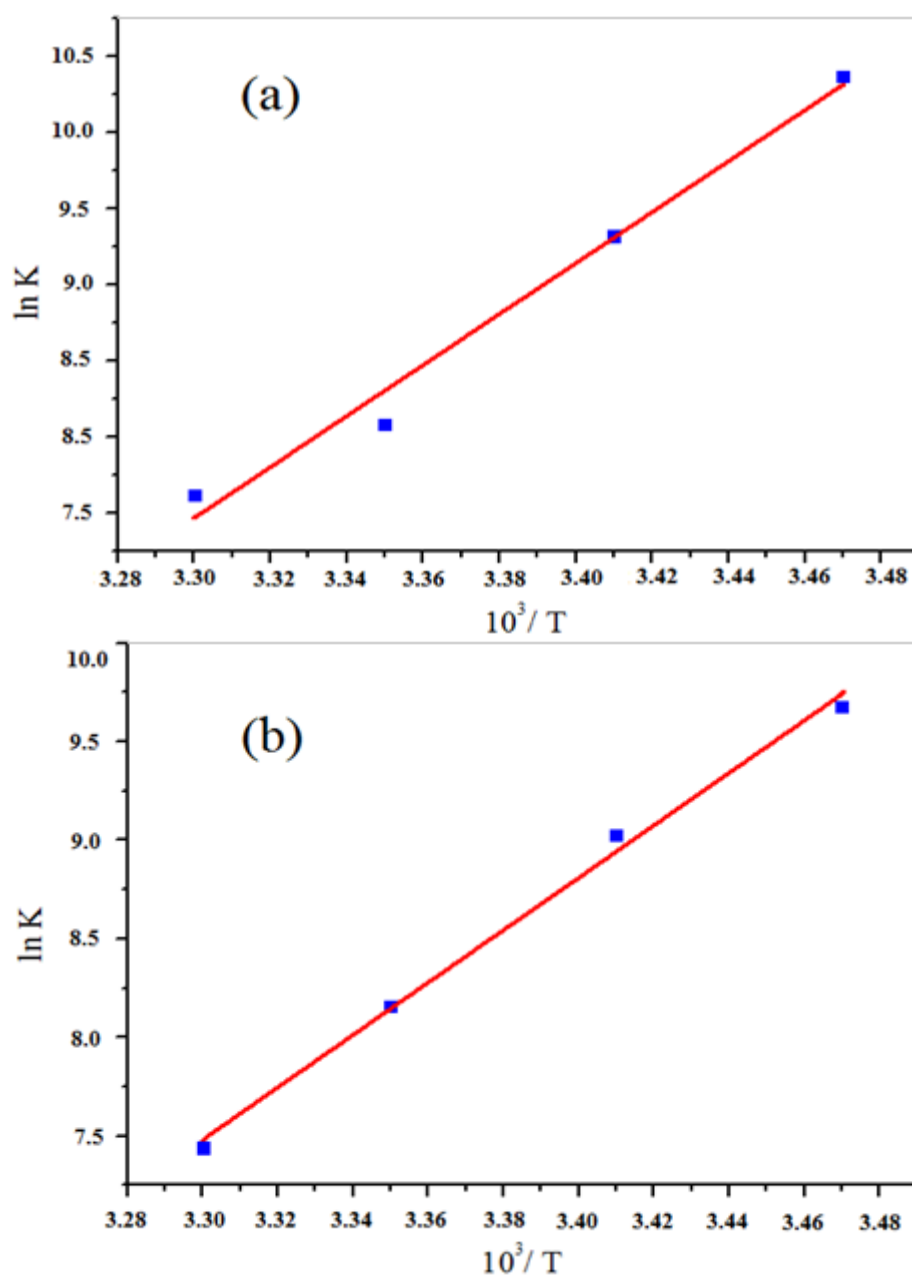


Figure 3. Van't Hoff plots for (a) SOZ- PiOH in chloroform, (b) SOZ- PiOH in dichloromethane.

Table 2. Experimental and predicted values of thermodynamic quantities for the CT complexation of N-(4-methoxyphenyl)-2-oxooxazolidine-3-sulfonamide with picric acid in chloroform and dichloromethane.

Parameter	In vacuum	Chloroform		Dichloromethane	
	Theoretical	Experimental	Theoretical	Experimental	Theoretical
ΔH (kJ/mol)	-168.3	-139	-134.50	-110.86	-122.36
ΔS (j/mol.k)	-586.88	-396.59	-364.98	-302.48	-334.52
ΔG (kJ/mol)	5.67	-20.81	-25.68	-20.72	-22.62
f	—	39.90	—	3.10	—
E_{CT} (eV)	—	3.04	—	3.75	—
μ_{EN} (D)	—	21.84	—	4.77	—
I_D (eV)	—	9.51	—	10.38	—

4. Determination of the Ionization Potential of the Donor

Belferragui et al. used Aloisi and Pignataro's equation to determine the ionization potential of the donor (I_D) in a CT complex: ⁴⁴

$$I_D (eV) = 5,76 + 0,153 \times 10^{-3} \nu_{CT} \quad (5)$$

where ν_{CT} is the wavenumber in cm^{-1} of the complex which corresponds to bands from the interactions between acceptor and donor molecules in the formed CT. Ionization potential is used to evaluate the electron-donating power of a donor molecule, which is the energy required to remove an electron from the highest occupied molecular orbital. The calculated ionization potentials are listed in **Table 2**.

5. Determination of Oscillator Strength (f) and Transition Dipole (μ_{EN})

Oscillator strength (f) is a dimensionless parameter, used to express the probability of CT band transitions. ⁴⁵ We can determine oscillator strength from the absorption spectra of the CT complexes; this quantity is calculated using the basic formula:

$$f = 0,432 \times 10^{-8} \int \epsilon dv \quad (6)$$

where $\int \epsilon dv$ is the area below the curve of the molar

extinction coefficient of the absorption band vs. frequency. As a first approximation, we obtain:

$$f = 0,432 \times 10^{-8} \epsilon_{CT} \Delta \nu_{1/2} \quad (7)$$

where ϵ_{CT} is the maximum molar extinction coefficient of the band and $\Delta \nu_{1/2}$ is the width of the band at half maximum. The oscillator strength is recalculated in **Table 2**. These values reflect the existence of interactions between the acceptor-donor pair with a relatively high probability of CT transitions. This is also supported by the relatively high heat of formation. The relationship between the extinction coefficient and the transition dipole was estimated using the following equation:

$$\mu_{EN} = 9,52 \times 10^{-2} \cdot \left[\frac{\epsilon_{CT} \Delta \nu_{1/2}}{\Delta \nu} \right]^{1/2} \quad (8)$$

where $\Delta \nu \approx \nu_{CT}$ at ϵ_{CT} and is defined as

$$-e \int \psi_{ex} \sum_i r_i \psi_g d\tau \cdot \mu_{EN}$$

6. IR spectra of CT complexes and reactants

The IR spectra of PiOH, SOZ and their corresponding CT complex are presented in **Fig. 4**, whereas their peak assignments are listed in **Table 3**.

Table 3. Assignments and frequencies (cm^{-1}) for picric acid, N-(4-methoxyphenyl)-2-oxooxazolidine-3-sulfonamide and their complex. ^{46,47}

PiOH	SOZ	SOZ/ PiOH complex (experimental)	Assignments
	3291 s	3277 s	$\nu(\text{N-H})$
3103 s		3094 m	$\nu(\text{O-H})$
2981 m	2966 w	2954 w	$\nu(\text{C-H})$ aromatic
	2842 w	2830 w	$\nu(\text{C-N})$
1861 w		1887 w	$\nu(\text{NO}_2)$
	1758 s	1745 s	$\nu(\text{N-H})$ deformation
1632 m	1608 s	1620 w	$\nu(\text{C=C})$
1527 s	1649 m	1596 m	phenyl breathing modes
1431 m	1511 m	1499 s	$\nu(\text{C-C}),$
1342 s	1402 w	1392 m	C-H in plane bend
	1358 m	1346 m	$\nu(\text{SO}_2)$
1148 w	1253 m	1241 m	C-H deformation
1087 w	1180 m	1138 m	C-H bend
919 m	1032 m	1019 w	C-H out of plane bend
704 s	963 w	907 w	
582 w	620 m	608 m	

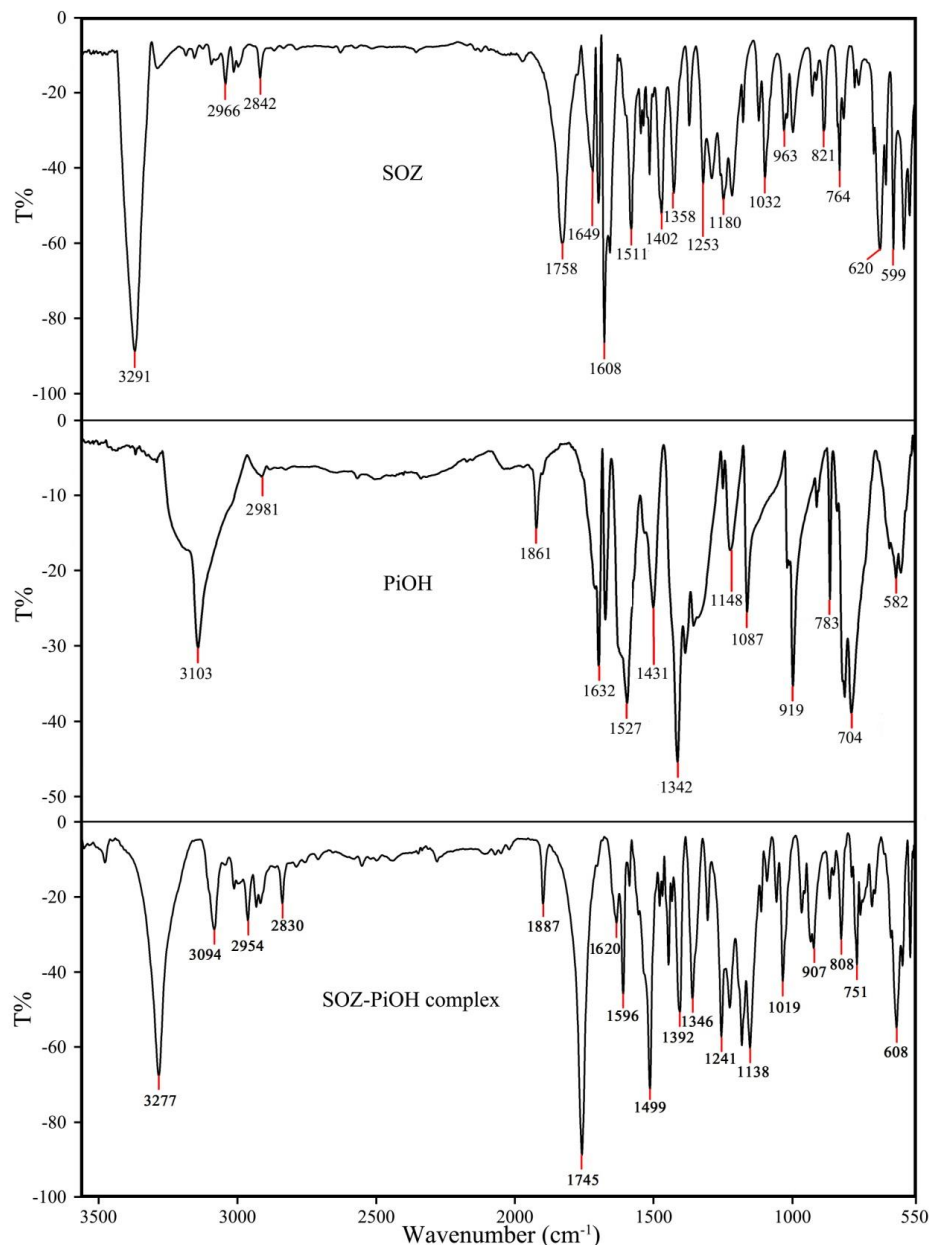


Figure 4. IR spectra for (a) picric acid, (b) N-(4-methoxyphenyl)-2-oxooxazolidine-3-sulfonamide, and (c) the SOZ-PiOH complex.

During formation of the CT complex, we observed the existence of free PiOH and SOZ in the spectrum of the SOZ-PiOH complex. However, the characteristic bands for SOZ and PiOH were shifted to lower frequencies in the SOZ-PiOH complex. These changes reflect the charge transfer between SOZ and PiOH on complexation.

Interestingly, the peaks for $\nu(\text{O-H})$ (3103 cm^{-1}), $\nu(\text{NO}_2)$ (1861 cm^{-1}) and $\nu(\text{C=C})$ (1632 cm^{-1}) in the free acceptor PiOH shifted to higher frequencies in the SOZ-PiOH complex: 3094 cm^{-1} , 1887 cm^{-1} and 1620 cm^{-1} respectively.

In addition, $\nu(\text{N-H})$ (3291 cm^{-1}) and $\delta(\text{N-H})$ (1758 cm^{-1}) in the free SOZ were higher than their corresponding peaks in the SOZ-PiOH complex,

where they appeared at 3277 cm^{-1} and 1745 cm^{-1} , respectively. The N-H peak intensity in SOZ-PiOH increased with respect to that in the free SOZ.

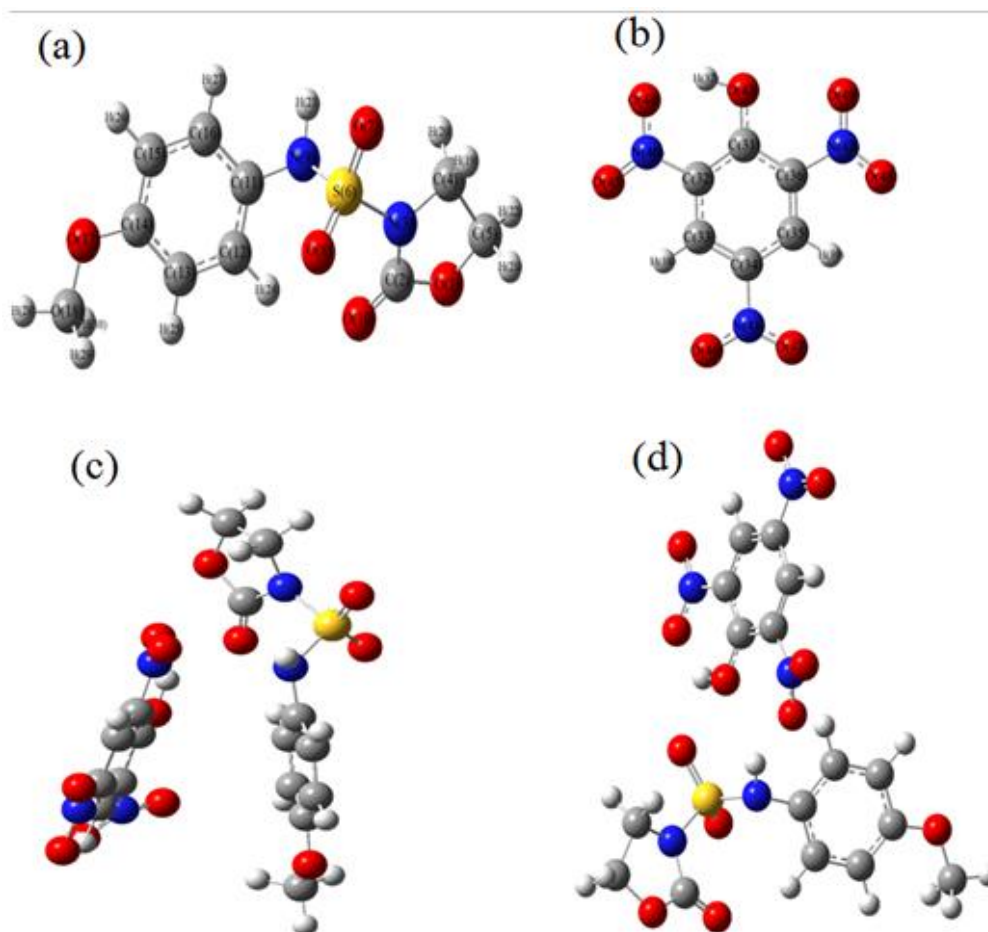
The abovementioned changes in the frequencies of the characteristic bands of free PiOH and free SOZ upon complexation supports the formation of a CT complex between SOZ and PiOH through the $\text{N}\cdots\text{H}\cdots\text{O}$ interaction.⁴⁸⁻⁵⁰

7. Molecular Modelling Studies

To obtain a better understanding about the process of charge transfer, we have complemented the experimental study on the SOZ-PiOH interaction with quantum chemical calculations using the Density Functional Theory (DFT) and Time Dependent

Table 4. Mulliken's electronic charge on various atoms of picric acid, N-(4-methoxyphenyl)-2-oxo-oxazolidine-3-sulfonamide and the picric acid/N-sulfamoyloxazolidinone complex using DFT (311G (d, p) basis set) calculations.

Atom Number	Mulliken's electronic charge (a.u) on different atoms in SOZ (a.u)	Mulliken's electronic charge (a.u) on different atoms in PiOH (a.u)	Mulliken's electronic charge (a.u) on different atoms in the CT-complex (a.u)	Difference (a.u)
S6	1.341	—	1.354	0.013
O7	-0.536	—	-0.569	-0.033
O8	-0.482	—	-0.481	0.001
N9	-0.787	—	-0.827	-0.040
C11	0.259	—	0.269	0.010
C12	-0.162	—	-0.152	0.010
C18	—	0.334	0.355	0.021
C31	—	0.251	0.229	-0.022
C32	—	-0.182	-0.164	0.018
C34	—	0.277	0.272	-0.005
C35	—	-0.180	-0.179	0.001
C36	—	0.235	0.233	-0.002
O43	—	-0.575	-0.629	-0.054
Dipole moment	3.537	1.905	2.989	—

**Figure 5.** Optimized geometric structures obtained using B3LYP of (a) N-(4-methoxyphenyl)-2-oxooxazolidine-3-sulfonamide, (b) picric acid, (c) the parallel model complex and (d) the T shape model complex

Density Functional Theory (TD-DFT) calculations at the B3LYP level.

7.1. Optimization of Geometries and Charge Distribution

The geometries of SOZ, PiOH and the SOZ-PiOH complexes were optimized under vacuum (**Fig. 5**). The binding energies values calculated at the DFT (B3LYP) level of the optimized configurations obtained from the two models previously described were **-6.957 kcal/mol** (perpendicular model) and **-6.767 kcal/mol** (parallel model), indicating that the first model was more stable and energetically favourable than the second.⁵¹

The calculated dipole moments of SOZ and PiOH were: 3.537 D and 1.905 D, respectively, while the same for the molecular complex was found to be 2.989 D (**Table 4**). This change in the dipole moment value indicates the charge transfer from SOZ to PiOH⁵². The electronic charge values for the **N9**, **C11** and **C12** atoms in the SOZ molecule were found to be -0.787, 0.259 and -0.162 a.u., respectively. The charges on the CT-complex with PiOH were found to change from atom to atom, as detailed in **Table 1**. The charges for **N9**, **C11**, **C31** and **O43** were found to have decreased in the CT complex, while the charges for **C12**, **C18** and **C32** had increased. The difference in charge values varied between -0.054 and 0.022 a.u. and the largest differences were found in the **N9** and

O34 atoms. This reflects the transfer of an observable quantity of electronic charge between SOZ and PiOH.

7.2. Correlation of Electronic Spectra with Spectroscopic Transitions

The UV-visible spectra of PiOH, SOZ and the PiOH-SOZ complex in chloroform are displayed in **Fig. 1**. These show that a new band appeared at 408 nm when PiOH and SOZ were mixed together; this broad band is related to the solvent polarity, which indicates the charge transfer nature of the complex. In order to gain greater understanding of electronic transitions taking place in the complex, we performed TD-DFT calculations for SOZ, PiOH and the SOZ-PiOH complex using a PCM model with the B3LYP/6-311G(d, p) method and chloroform as solvent. The energy and oscillator strength values obtained from TD-DFT calculations for the SOZ-PiOH complex in transitions occurring at particular wavelengths are shown in **Table 5**. In the experimental visualization, the new peak's maximum appeared at 408 nm in chloroform and 331 nm in dichloromethane, while the predicted peak maximum values were at 481 nm and 407 nm in chloroform and dichloromethane, respectively. Thus, the absorption maxima of the charge transfer elucidated in the present theoretical investigation TD-B3LYP/6-311G(d, p) for the PCM model corroborated well with the experimental results, with a deviation of 73 – 76 nm.

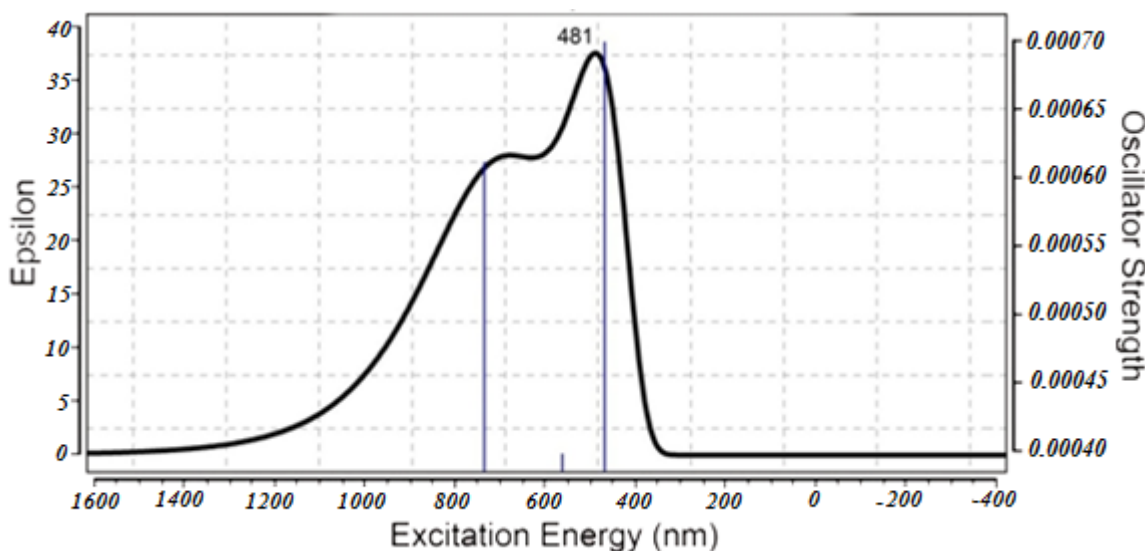


Figure 6. Computed absorption spectra of SOZ, PiOH and the SOZ-PiOH CT complex in chloroform using TD-DFT.

Table 5. Results of TD-DFT calculations for the SOZ-PiOH complex in a PCM model using chloroform, dichloromethane and methanol as solvent

Solvent	Transition	Wavelength (nm)	Oscillator strength	Energy (eV)	Experimental λ_{\max} (nm)
CHCl ₃	HOMO→LUMO	641.88	0.0006	1.93	408
	HOMO→LUMO+1	528.28	0.0004	2.34	
	HOMO→LUMO+2	481.75	0.0007	2.57	
	HOMO-1→LUMO	408.84	0.0006	3.03	
	HOMO-1→LUMO+1	359.71	0.0007	3.44	
	HOMO-2→LUMO	338.68	0.0147	3.66	
CH ₂ Cl ₂	HOMO→LUMO	611.58	0.0006	2.02	331
	HOMO→LUMO+1	508.49	0.0004	2.43	
	HOMO→LUMO+2	407.68	0.0007	2.65	
	HOMO-1→LUMO	395.81	0.0006	3.13	
	HOMO-1→LUMO+1	350.05	0.0008	3.54	
	HOMO-3→LUMO	334.54	0.0657	3.70	

7.3. Predicted Thermodynamic Parameters

For further confirmation of the charge transfer complex (SOZ-PiOH) formation, we calculated the thermodynamic parameters by molecular modelling using the B3LYP/6-311G (d, p) method in vacuum, chloroform and dichloromethane. The thermodynamic parameter values are listed in **Table 2**. The thermodynamic results obtained under vacuum were larger than those in chloroform and dichloromethane. This is due to the solvent effect and the dielectric constant (in vacuum $\epsilon=0$).

We observed that the complexation was an exothermic reaction justified by the negative enthalpy change (ΔH) suggesting that in nature, the complexation process is an enthalpy driven.

Additionally, the enthalpy change of the complex in chloroform was more negative than in dichloromethane, which indicates that the acceptor and donor interactions were stronger in chloroform than in dichloromethane. The change of free energy (ΔG) was negative; thus the charge transfer is a spontaneous reaction.

The thermodynamic quantities obtained by experimental methods were compared with those obtained theoretically, and we found that the results were of the same sign and magnitude, with differences of less than 32.04 kJ/mol. This indicates good accord between experimental and theoretical results.

7.4. Simulated IR Spectra

The predicted band assignments for SOZ, PiOH and the SOZ-PiOH complex (**Table 3**) were obtained

using B3LYP/6-311G(d, p). The main IR bands of SOZ and PiOH were present in the spectrum of the complex, with changes in intensities or wavenumbers of vibrational bands implying its formation (**Fig. 7**).

N—H Vibrations:

The stretching vibration of the amino group (N-H) in the SOZ-PiOH complex was present as a very strong and broad band at 3277 cm⁻¹ in the experimental IR spectra, while the corresponding computed peak appeared at 3188 cm⁻¹. These results show good agreement between experimental and theoretical IR spectra, with a deviation of only 89 cm⁻¹.

O—H Vibrations:

The hydroxyl group (O—H) vibration appeared at 3094 cm⁻¹ as a strong band near the vibration of the amino group in the experimental IR. The same vibration was calculated at 3153 cm⁻¹, which is in good accord with the experimental data.

Aromatic C-H, SO₂ and NO₂ Vibrations:

In aromatic compounds, the ν_{C-H} generally appears in the range of 3000-3100 cm⁻¹.⁵³⁻⁵⁶ In this study, the aromatic stretching band appeared at 2954 cm⁻¹ while the corresponding theoretical wavenumber was determined to be 3076 cm⁻¹.

As for other peaks, we noticed that the experimental peaks of SO₂ and NO₂ appeared at 1346 cm⁻¹ and 1887 cm⁻¹, respectively. However, in the calculated IR spectra they appeared at 1308 cm⁻¹ and 2021 cm⁻¹.

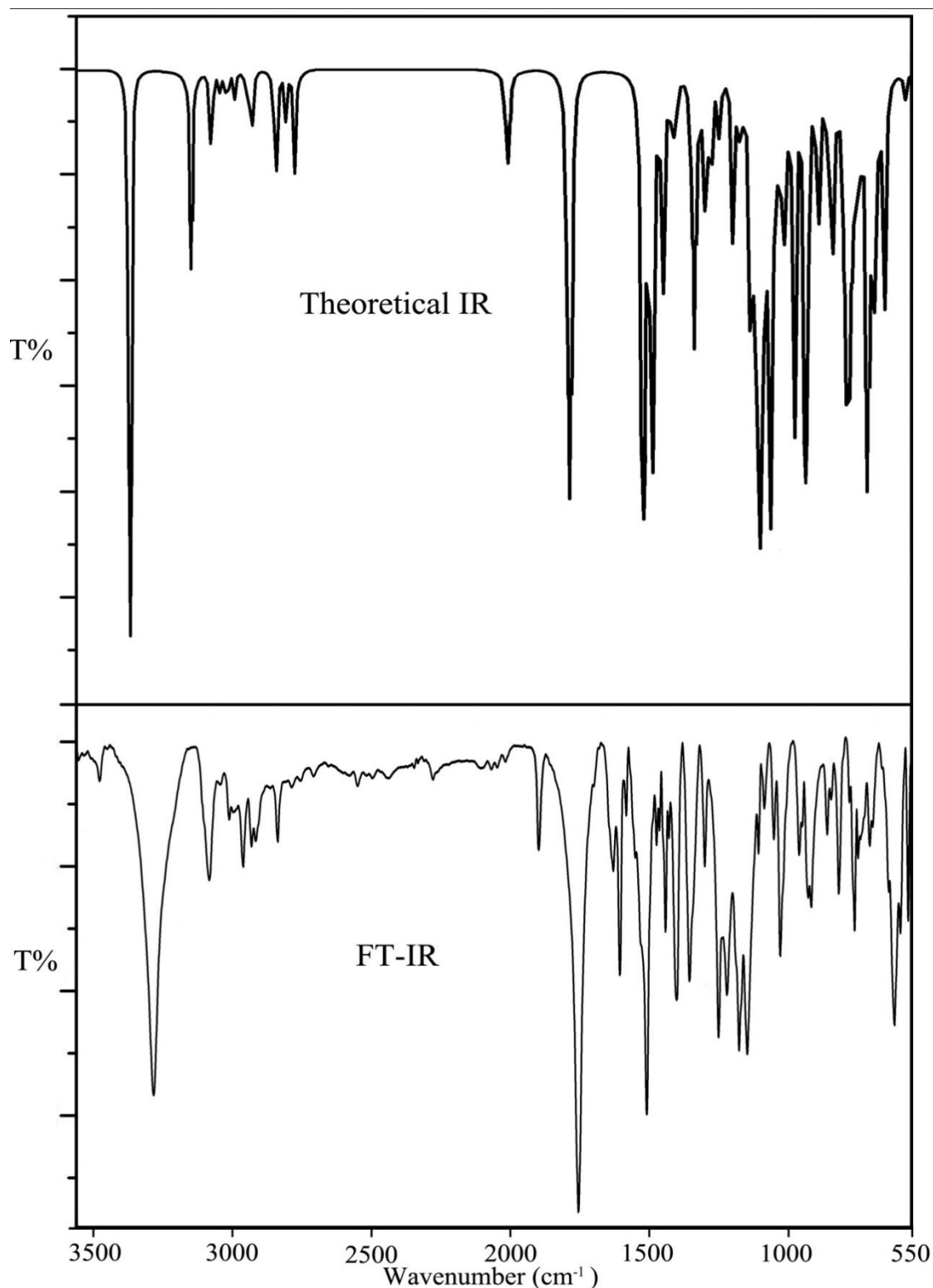


Figure 7. Experimental and simulated IR spectra of the SOZ-PiOH complex.

These deviations between experimental and calculated infrared frequencies were justified by the fact that the IR spectra was carried out experimentally in the solid state while the calculated spectra were for the compounds in gas phase.

7.5. HOMO-LUMO calculations for the SOZ-PiOH Complex at Ground State

The HOMO (the Highest Occupied Molecular Orbital) and LUMO (the Lowest Unoccupied Molecular

Orbital), also called FMO (Frontier Molecular Orbitals), are the most likely orbitals to be involved in chemical reactivity, and play significant roles in electronic spectra, as well as in interactions between molecules.^{57,58} The computed energies of HOMO orbitals and their localization and appearance in the model structures are suggestive of the efficiency of the charge transfer between acceptor and donor molecules.

A range of LUMO and HOMO values for the PiOH-SOZ complex in the ground state was obtained using DFT at the B3LYP level, and these are illustrated in **Fig. 7**. It is evident from the figure that LUMOs were generally delocalized over the PiOH molecule, while HOMO and HOMO-1 were localized only on the SOZ. Thus the 408 nm band

corresponds to HOMO (PiOH) and to LUMO+2 (SOZ) in chloroform, while the 331 nm band corresponds to the same transition in dichloromethane. This is a picture of the molecular orbital level for the CT transition taking place in this complex. The energy values for HOMO, HOMO-*n*, LUMO and LUMO-*n*, where *n* = 1 to 5 for PiOH, SOZ and the PiOH-SOZ complex in ground state are provided in **Table 6**. It is interesting to note that the LUMO energy level of the PiOH-SOZ CT complex (-5.632 eV) compared well with the LUMO energy level of PiOH (-3.918 eV), while the HOMO energy level (-8.326 eV) of the complex was close to the HOMO energy level of PiOH (-8.727 eV). This trend for localization of frontier molecular orbitals in the PiOH-SOZ system is very similar to other electron donor-acceptor composite systems.^{59,60}

Table 6. HOMO-LUMO energies for picric acid, N-(4-methoxyphenyl)-2-oxooxazolidine-3-sulfonamide and the CT complex at ground state. Orbital numbers are written in brackets.

Orbital	Orbital energy (eV)		
	Picric acid	N-sulfamoyloxazolidinone	CT complex
HOMO	-8.727 (58)	-5.796 (71)	-8.326 (129)
HOMO-1	-8.489 (57)	-6.911 (70)	-8.816 (128)
HOMO-2	-8.762 (56)	-7.619 (69)	-9.006 (127)
HOMO-3	-9.006 (55)	-8.000 (68)	-9.578 (126)
HOMO-4	-9.034 (54)	-8.245 (67)	-9.741 (125)
HOMO-5	-9.143 (53)	-8.517 (66)	-9.796 (124)
LUMO	-3.918 (59)	-0.108 (72)	-5.632 (130)
LUMO+1	-3.292 (60)	-0.054 (73)	-5.197 (131)
LUMO+2	-2.993 (61)	0.462 (74)	-4.898 (132)
LUMO+3	-0.952 (62)	0.979 (75)	-4.517 (133)
LUMO+4	-0.653 (63)	1.768 (76)	-4.027 (134)
LUMO+5	0.789 (64)	1.986 (77)	-2.857 (135)

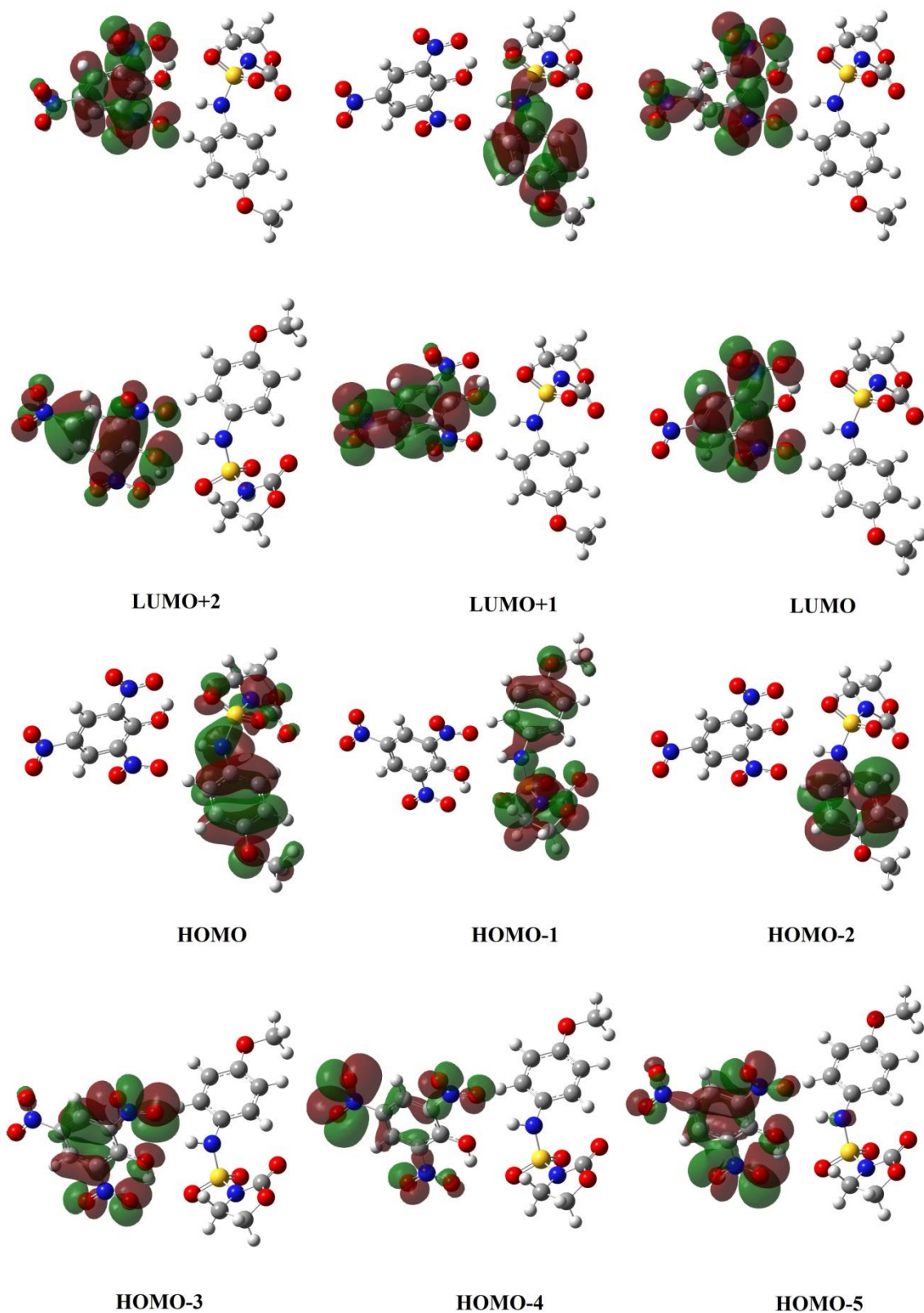


Figure 8. Calculated FMO pictures of the SOZ-PiOH complex using the DFT method.

Table 7. SOZ-PiOH interactions and stabilization energies in a perpendicular model of the CT complex by the B3LYP method.

Donor	Acceptor	$E^{(2)}$ (kcal/mol)	Distance (Å)	Angle (°)
<i>From SOZ to PiOH</i>				
LP(2) O7	BD*(1) C31-O43	0.16	2.719	154.73
LP(3) O7	BD*(1) C31-O43	0.12	2.719	154.73
<i>From PiOH to SOZ</i>				
LP(1) O43	BD*(1) N9-H23	2.42	2.338	143.26
LP(2) O43	BD*(1) N9-H23	0.42	2.338	143.26
LP(1) O45	BD*(1) N9-H23	1.46	2.387	146.98
LP(2) O45	BD*(1) N9-H23	0.92	2.387	146.98

BD(1) = σ bonding orbital; BD(1)* = σ^* antibonding orbital; LP(1) and LP(2) indicates 1st and 2nd lone pair electron, respectively. $E^{(2)}$ = stabilization energy.

From the above, it is evident that orbital interaction energy arises mainly from the charge transfer between occupied and unoccupied orbitals.

7.6. Natural Bond Orbital (NBO) Analysis

The Natural Bond Orbital (NBO) approach of Weinhold et al. has been frequently used in the estimation of intra- and intermolecular interactions.⁶¹ It provides a convenient basis for investigating charge transfers or conjugative interactions in molecular systems. NBO analysis was used to provide the electronic wave-functions that are interpreted in a set of occupied Lewis orbitals, the contribution of atomic orbitals and a set of non-Lewis localized orbitals. The electronic delocalization interaction can be quantitatively represented using the energy of stabilization ($E^{(2)}$), which can be expressed as equation (9):⁶²⁻⁶⁵

$$E^{(2)} = -\frac{\langle \sigma | F | \sigma \rangle}{\varepsilon_{\sigma^*} - \varepsilon_{\sigma}} \times n_{\sigma} = -\frac{F_{ij}^2}{\Delta E} \times n_{\sigma} = -\frac{F_{ij}^2}{E_j - E_i} \times n_{\sigma} \quad (9)$$

where $\langle \sigma | F | \sigma \rangle$ or F_{ij}^2 is the Fock matrix element between the i and j NBO orbitals, F_{ij} represents the off-diagonal NBO Fock matrix element, ε_{σ^*} and ε_{σ} denote the energies of the σ and σ^* NBO orbitals, n_{σ} is the population of the donor σ orbital, while E_i and E_j are the diagonal elements (orbital energies).

The energies of stabilization $E^{(2)}$ of the CT complex calculated using the RB3LYP/6-31G (d) single point method, and the geometric parameters of the formed hydrogen bond in the SOZ-PiOH complex are presented in **Table 7**. It is known that the energies of strong H-bonds vary between 1 and 10 kcal/mol, whereas the energies of weak H-bonds are lower than 2 kcal/mol.⁶⁶

In this study, we found that the N9-H23 bond was the centre of electron density, and the O43 atom in PiOH was classified as the best electron acceptor location, with an $E^{(2)}$ value of 2.42 kcal mol⁻¹, thus this hydrogen bond was fairly strong. Consequently, we suggest a formula which can explain the hydrogen bonding between SOZ and PiOH.⁶⁷⁻⁶⁹

7.7. Molecular Electrostatic Potential (MEP)

MEP values are very helpful in determining sites for electrophilic attack and nucleophilic reactions, especially H-bonding interactions, and are related to electronic density.⁷⁰⁻⁷² The map created by these calculations can visualize the charged regions of a molecule. Charge distributions are used to determine interactions between molecules. The electrostatic potential values are represented by different colours: the most electronegative potential regions are depicted in red, while regions of most positive electrostatic potential are in blue and regions of zero potential in green. So the potential decreases as follows: blue > green > yellow > orange > red. The MEP values for SOZ, PiOH and their CT complex were calculated at the B3LYP (6-31G (d)) level (**Fig. 9**). The map plot for free SOZ (**Fig. 9 (a)**) demonstrates that the most positive potential (blue) was localized on the amino group corresponding to a map surface value of 0.055 a.u., and became more positive in the SOZ-PiOH CT-complex (0.093 a.u.) (**Fig. 9 (c)**). The negative potential (red) of the free SOZ was observed around the sulfonyl group with a maximum surface value of -0.055 a.u., but in the CT-complex it was more negative (-0.086 a.u.). For the acceptor, we observed that the positive region of the free PiOH was focused in the centre of the benzene moiety (**Fig. 9 (b)**), with a maximum surface map value of 0.052 a.u., whereas the regions of negative potential were observed around the nitrogen groups and the hydroxyl moiety with a maximum surface value of -0.052 a.u. This indicates

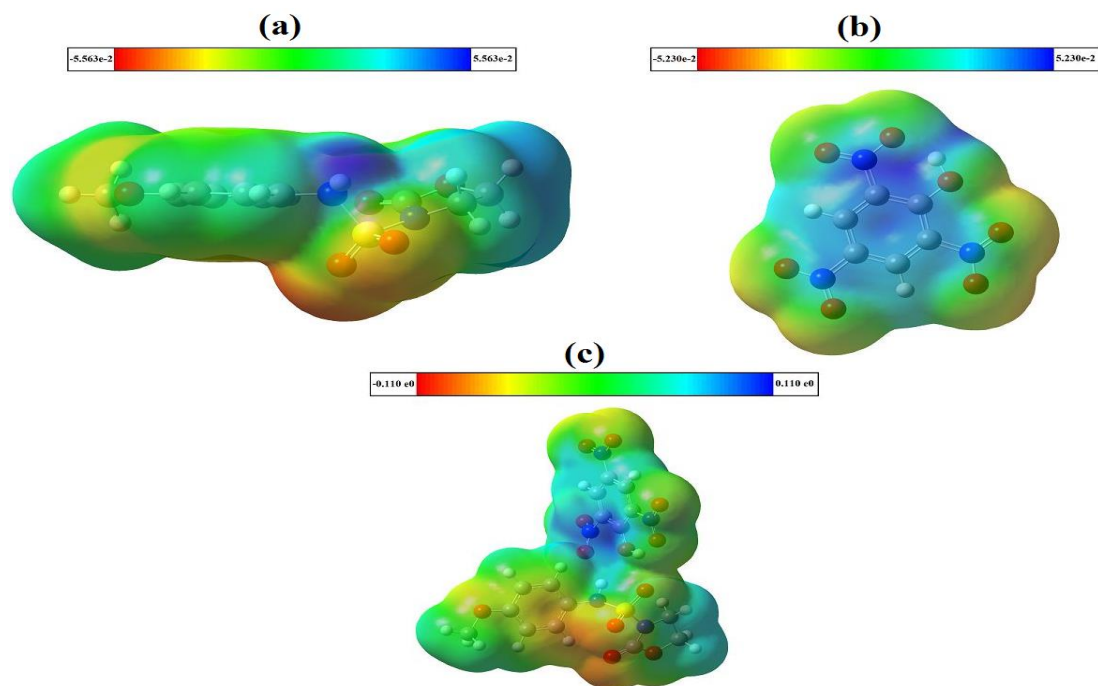


Figure 9. Molecular electrostatic potential map of (a) SOZ, (b) PiOH, (c) the SOZ-PiOH complex.

that the electronic cloud delocalized from SOZ (donor) to PiOH (acceptor), as confirmed by the FTIR study and NBO analysis.^{70,73}

CONCLUSION

The CT complex formed by a 1:1 stoichiometry ratio of N-(4-methoxyphenyl)-2-oxooxazolidine-3-sulfonamide as donor and picric acid as acceptor was investigated in two different polar solvents. The study revealed that the stability constants of the SOZ-PiOH complexes increased with decreasing solvent polarity. The complex dissociated in polar solvents because of their large dielectric constants. The thermodynamic parameters as determined by both spectroscopic measurements and theoretical calculations showed that the charge-transfer complexation reaction was exothermic and enthalpy-entropy co-driven. The TD-DFT method was also used to investigate the geometric structure of the CT complex. The results obtained indicated an $n \rightarrow \sigma^*$ transition and the formation of N---H---O H-bonds between the acceptor and donor molecules. The modelling results thus corroborated well with the experimental data.

ACKNOWLEDGEMENTS

The authors acknowledge the Minister of the High Education and Scientific Research of Algeria, this work was supported by DGRST through project PRFU B00L01UN240120190001.

REFERENCES

1. McGlynn, S. P. (1958) *Chem. Rev.*, **58**, 1113–1156.
2. Foster, R. (1969) *Organic Charge-transfer Complexes*. Academic Press, New York,
3. Mulliken, R. S., Person, W. B. (1969) *Molecular complexes*. Wiley, New York.
4. Hanna, M. W., Lippert, J. L. (1973) *Molecular Complexes*. Ed R Foster, Elek Science. London.
5. Ahuja, S. (2000) *Chiral Separation by Chromatography*, Oxford university Press. Washington,
6. Rosen, B. M., Wilson, C. J., Wilson, D. A., Peterca, M., Imam, M. R., Percec, V. (2009) *Chem. Rev.*, **109**, 6275–6540.
7. Matsumura, K., Mori, T., Inoue, Y. (2010) *J. Org. Chem.*, **75**, 5461–5469.
8. Chanon, M., Hawley, M. D., Fox, M. A., Fox, M. A. (1988) *Photoinduced Electron Transfer*. Eds M. Chanon, Elsevier, New York.
9. Zhuang, X. -D., Chen, Y., Li, B. -X., Ma, D. -G., Zhang, B., Li, Y. (2010) *Chem. Master.*, **22**, 4455–4461.
10. Faulques, E., Perry, D. L., Yeremenko, A. V. (2004) *Spectroscopy of Emerging Materials*. Kluwer Academic Publishers, Boston.
11. Wang, C., Dong, H., Hu, W., Liu, Y., Zhu, D. (2012) *Chem. Rev.*, **112**, 2208–2267.
12. Wang, W., Luo, L., Sheng, P., Zhang, J., Zhang, Q. (2021) *Chem-Europ. J.*, **27**(2), 464–490.

13. Sue, C. -H., Basu, S., Fahrenbach, A. C., Shveyd, A. K., Dey, S. K., Botrosac, Y. Y., Stoddart, J. F. (2010) *Chem. Sci.*, **1**, 119–125.
14. Lee, S. K., Shin, S. Y., Lee, S., Lee, C., Park, J. W. (2001) *J. Chem. Soc., Perkin Trans.*, **2**, 1983–1988.
15. Han, J., Yang, D., Jin, X., Jiang, Y., Liu, M., Duan, P. (2019) *Angew. Chem.*, **131(21)**, 7087–7093.
16. Arnold, B. R., Euler, A., Fields, K., Zaini, R. Y. (2000) *J. Phys. Org. Chem.*, **13**, 729–734.
17. Sun, J., Yang, S., Wu, J., He, X., Zhang, Y., Ji, J., Zhang, C., Liang, Z. (2022) *Chem. Engin. J.*, **428**, 132625.
18. Barman, D., Gopikrishna, P., Lyer, P. K. (2021) *Languir.*, **37(26)**, 8024–8036.
19. Hacker, C. A., Pookpanratana, S., Jurchescu, O. D. (2022) *Material Horizon*, **9(1)**, 271–280.
20. Li, M. -H., You, M. H., Lin, M. -J. (2021) *Dalton. Transact.*, **50(39)**, 13961–13967.
21. Linstrom, P. J., Mallard, W. G. (2001) *The NIST Chemistry WebBook*, **46**, 1059–1063.
22. Wang, Y. -J., Feng, L. -Y., Zhai, H. -J. (2019) *Phys. Chem. Chem. Phys.*, **21(33)**, 18338–18345.
23. Abdaoui, M., Dewynter, G., Toupet, L., Montero, J. L. (2000) *Tetrahedron.*, **56**, 2427–2435.
24. Dinar, K., Sahra, K., Seridi, A., Kadri, M. (2014) *Chem. Phys. Lett.*, **595-596**, 113–120.
25. Berredjem, M., Regainia, Z., Djahoudi, A., Aouf, N. D., Dewynter, G., Montero, J. L. (2000) *Phosphorus. Sulfur. Silicon.*, **165**, 249–264.
26. Dewynter, G., Abdaoui, M., Regainia, Z., Montero, J. L. (1996) *Tetrahedron.*, **52**, 14217–14224.
27. Belfaragui, M., Seridi, A., Winum, J. -Y., Abdaoui, M., Kadri, M. (2013) *Spectrochim. Acta Part A: Mol. Biomol. Spectrosc.*, **108**, 55–61.
28. Kadri, M., Djemil, R., Abdaoui, M., Winum, J. -Y., Cautrot, F., Montero, J. -L. (2005) *Bioorg. Med. Chem. Lett.*, **15**, 889–894.
29. AlRabiah, H., Abdel-Aziz, H. A., Mostafa, G. A. E. (2019) *J. Mol. Liq.*, **286**, 110754.
30. Frisch, M. J., Trucks, G. W., Schlegel, H. B., Scuseria, G. E., Robb, M. A., Cheeseman, J. R., Scalmani, G., Barone, V., Mennucci, B., Petersson, G. A., Nakatsuji, H., Caricato, M., Li, X., Hratchian, H. P., Izmaylov, A. F., Bloino, J., Zheng, G., Sonnenberg, J. L., Hada, M., Ehara, M., Toyota, K., Fukuda, R., Hasegawa, J., Ishida, M., Nakajima, T., Honda, Y., Kitao, O., Nakai, H., Vreven, T., Montgomery Jr., J. A., Peralta, J. E., Ogliaro, F., Bearpark, M., Heyd, J. J., Brothers, E., Kudin, K. N., Staroverov, V. N., Kobayashi, R., Normand, J., Raghavachari, K., Rendell, A., Burant, J. C., Iyengar, S. S., Tomasi, J., Cossi, M., Rega, N., Millam, J. M., Klene, M., Knox, J. E., Cross, J. B., Bakken, V., Adamo, C., Jaramillo, J., Gomperts, R., Stratmann, R. E., Yazyev, O., Austin, A. J., Cammi, R., Pomelli, C., Ochterski, J. W., Martin, R. L., Morokuma, K., Zakrzewski, V. G., Voth, G. A., Salvador, P., Dannenberg, J. J., Dapprich, S., Daniels, A. D., Farkas, Ö., Foresman, J. B., Ortiz, J. V., Cioslowski, J. and Fox, D. J. (2009) *Gaussian. Inc.*, Wallingford CT.
31. Seridi, S., Dinar, K., Seridi, A., Berredjem, M. and Kadri, M. (2016) *New J. Chem.*, **40**, 4781–4792.
32. Shehab, O. R., AlRabiah, H., Abdel-Aziz, H. A., Mostafa, G. A. E. (2018) *J. Mole. Liq.*, **257**, 42–51.
33. Lee, C., Yang, W., Parr, R. G. (1988) *Phys. Rev. B.*, **37**, 785.
34. Anton, G., Anton, K., Deyan, I., Deyan, D., Simeon, S., Lian, N., Dimana, N., Denitsa, Y. (2018) *Spectrochim. Act. A: Mole. Biomole Spect.*, **192**, 263–274.
35. Benesi, H. A., Hildebrand, J. H. (1949) *J. Am. Chem. Soc.*, **71**, 2703–2707.
36. Prabu, S., Samad, N. A. A., Ahmad, N. A., Jumbri, K., Raoov, M., Rahim, N. Y., Mohamad, S. (2020) *Carbohydr. Res.*, **497**, 108138.
37. Al-Humaidi, J. Y., El-Sayed, M. Y., Refat, M. S., Altalhi, T. A., Eldaroti, H. H. (2021) *J. Mol. Liq.*, **333**, 115928.
38. Pang, Y., Thomas, A., Nagaajan, K., Vergauwe, R. M., Joseph, K., Patrahau, B., Ebbesen Angew, T. (2020) *Chem. Inter. Ed.*, **59(26)**, 10436–10440.
39. Foster, R., Thomson, T. J. (1962) *Trans. Faraday. Soc.*, **58**, 860–868.
40. Rekharsky, M. V., Inoue, Y. (1998) *Chem. Rev.*, **98**, 1875–1918.
41. Inoue, Y., Hakushi, T., Liu, Y., Tong, L. H., Shen, B. J., Jin, D. S. (1993) *J. Am. Chem. Soc.*, **115**, 475–481.
42. Lima, E. C., Gomes, A. A., Tran, N. H. (2020) *J. Mol. Liq.*, **311**, 113315.

- 46 Karim Dinar, Mekki Kadri and Achour Seridi
- Charge Transfer Complex of N-(4-methoxyphenyl)-2-oxooxazolidine-3-sulfonamide and Picric Acid: Experimental and DFT Studies
43. Simoes-Cardoso, J. C., Yoshimoto, N., Yamamoto, S. (2019) *J. Chromat. A.*, **1608**, 460405.
44. Aloisi, G. G., Pignataro, S. (1973) *J. Chem. Faraday. Trans.*, **69**, 534–539.
45. Lever, A. B. P. (1985) *Inorganic Electronic Spectroscopy*, second ed. Elsevier, Amsterdam.
46. Shimanouchi, T. (1972) Table of Molecular Vibrational Frequencies Consolidated. **1(39)**, 164. *Nat. Stand. Ref. Data Ser, Nat. Bur. Stand (U. S.)*.
47. Lin-Vein, D., Colthup, N. B., Fateley, W. G., Grasselli, J. G. (1991) The Hand Book of Infrared and Raman Characteristic Frequencies of Organic Molecules, *Academic Press, San Diego*.
48. Adam, A. A., Refat, M. S. (2016) *Journal of Molecular Liquids*, **219**, 377–389.
49. Al-Ahmary, K. M., Alenezi, M. K. S., Habeeb, M. M. (2016) *Journal of Molecular Liquids.*, **220**, 166–182.
50. Miyan, L., Ahmad, A. (2016) *Journal of Molecular Liquids*, **219**, 614–623.
51. Suresh, G., Venkatesh, N., Naveen, B., Mahipal, V., Madhavi, N., Parthasarathy, T. (2020) *J. sol. Chem.*, **49(6)**, 777–797.
52. Abbu, V., Nampally, V., Baindla, N., Tigulla, P. (2019) *J. Sol. Chem.*, **48(1)**, 61–81.
53. Refat, M. S., Elfalaky, A., Elesh, E. (2011) *J. Mol. Struct.*, **990**, 217–226.
54. Silverstein, M., Clyton Basseler, G., Morill, C. (1981) *Spectrometric Identification of Organic Compounds*. Wiley, New York.
55. Sundaraganesan, N., Ilakiyamani, S., Joushua, B. D. (2007) *Spectrochim. Acta.*, **67**, 287–297.
56. Melek, H.; Chiraz, K.; Taha, G. (2017) *Bulletin of Materials Science*, **40**, 55–66.
57. Prasad, O., Sinha, L., Misra, N., Narayan, V., Kumar, N., Pathak, J. (2010) *J. Mol. Struct: Theochem.*, **940**, 82–86.
58. Miar, M., Shiroudi, A., Pourshamsian, K., Oliayy, A. R., Hatamjafari, F. (2021) *J. Chem. Res.*, **45(1-2)**, 147–158.
59. Mizuseki, H., Igarashi, N., Belosludov, R. V., Farajian, A. A., Kawazoe, Y. (2003) *Jpn. J. Appl. Phys.*, **42**, 2503–2506.
60. Mizuseki, H., Igarashi, N., Belosludov, R. V., Farajian, A. A., Kawazoe, Y. (2003) *Synth. Met.*, **138**, 281–283.
61. Frisch, A., Nielson, A. B., Holder, A. J. (2000) GAUSSVIEW User Manual. *Gaussian Inc, Pittsburgh, PA*.
62. Ureña, F. P., Avilés Moreno J. R., López González, J. J. (2012) *Tetrahedr. Asym.*, **23(6-7)**, 515–525.
63. Reed, A. E., Curtiss, L. A., Weinhold, F. (1988) *Chem. Rev.*, **88**, 899–926.
64. Chocholoušová, J., Špirko, V., Hobza, P. (2004) *Phys. Chem. Chem. Phys.*, **6**, 37–41.
65. Al-Ahmary, K. M., Habeeb, M. M., Aljahdali, S. H. (2019) *J. Mole. Liq.*, **277**, 453–470.
66. Uccello-Barretta, G., Balzano, F., Sicoli, G., Frígola, C., Aldana, I., Monge, A., Paolino, D., Guccione, S. (2004) *Bioorg. Med. Chem.*, **12**, 447–458.
67. Issa, Y. M., Abdel-Latif, S. A., El-Ansary, A. L., Hassib, H. B. (2021) *New. J. Chem.*, **45(3)**, 1482–1499.
68. Al-Ahmary, K. M., Moustafa, M. H., Safaa, H. A. (2019) *J. mol. Liq.*, **277**, 453–470.
69. Arulaabaranam, K., Muthu, S., Mani, G., Irfan, A. (2021) *J. mol. Liq.*, **341**, 116934.
70. Mansour, A. M. (2013) *J. Mol. Struct.*, **1035**, 114–123.
71. Rahuman, M. H., Muthu, S., Raajaraman, B. R., Raja, M., Umamahesvari, H. (2020) *Heliyon.*, **6(9)**, e04976.
72. Basha, F., Khan, F. L. A., Muthu, S., Raja, M. (2021) *Comput. Theor. Chem.*, **1198**, 113169.
73. Demircioğlu, Z., Kaştaş, G., Kaştaş, C. A., Frank, R. (2019) *J. mol. Struct.*, **1191**, 129–137.